Evolution of Cold Shock-Bounded Slabs

John M. Blondin [1] and Brian S. Marks [2]

Department of Physics, North Carolina State University, Raleigh NC 27695-8202

Abstract

The stability and evolution of cold, shock-bounded slabs is studied using numerical hydrodynamic simulations. We confirm the analysis of Vishniac[0], who showed that such slabs are unstable if they are perturbed by a displacement larger than their width. The growth rate of this nonlinear thin shell instability (NTSI) is found to increase with decreasing wavelength, in qualitative agreement with Vishniac's analysis. The NTSI saturates when the bending angle becomes large and the growth in the width of the slab pinches off the perturbation. After saturation, the slab remains greatly extended with an average density much less than the original slab density, supported primarily by supersonic turbulence within the slab. Linear perturbations are also found to be unstable in that they can lead to turbulent flow within the slab, although this response to linear perturbations is distinct from, and much less violent than the NTSI.

Keywords: hydrodynamics – shock waves – ISM: kinematics and dynamics – stars: formation – supernova remnants

1 Introduction

Numerical simulations of shock-bounded slabs – a planar slab of cold gas bounded on both sides by strong shocks – have shown such objects to be dynamically unstable. This phenomenon has been seen in simulations of molecular clouds[0], colliding stellar winds[0], and evolving stellar winds[0]. The nature of this instability was studied analytically by Vishniac[0], who showed that cold, shock-bounded slabs are stable to linear displacements, but unstable to nonlinear displacements. He thus coined the term Nonlinear Thin-Shell Instability (NTSI).

[1] 1996 Cottrell Scholar

[2] Currently address: Department of Engineering Sciences and Applied Mathematics, Northwestern University, Evanston IL 60208

The NTSI is applicable to any thin, dense (relative to the in-flowing gas) shell of gas bounded on both sides by shock waves. This situation arises naturally if both shocks are strongly radiative, i.e., if the post shock gases radiate away all the shock-generated thermal energy in a distance much less than the size of the slab. This situation typically requires supersonic flow in relatively dense media such that the post shock cooling length, inversely proportional to the density, is small compared to other characteristic lengths of the system.

Examples might include colliding stellar winds in close hot star binaries[0], the interaction of a single time-varying wind as in the evolution of massive stars[0], supersonic flows in molecular clouds leading to star formation[0], the onset of radiative cooling in supernova remnants[0], the collision of clouds moving in a protogalactic environment leading to the formation of globular clusters[0], and the gravitational collapse of cosmological sheets in the formation of galaxies[0].

In this paper we use numerical simulations to confirm the analysis of the NTSI by Vishniac[0], and to study the long-term behavior of shock-bounded slabs. In §2 we describe the idealized shock-bounded slab with which we have studied the NTSI, and our numerical techniques for simulating the evolution of such an idealized slab. In §3 we describe the evolution of the NTSI, and we discuss the role of the NTSI in various astrophysical systems in §4.

2 The Idealized Shock-Bounded Slab

To investigate the NTSI we consider a planar shock-bounded slab of gas described by an isothermal equation of state, $P = a^2\rho$, where P, ρ, and a are the pressure, density, and sound speed of the gas, respectively. Uniform flow approaches the planar slab from both sides with a velocity V_e and density ρ_e. As shocked material accumulates in the slab, the bounding shocks move outward with a velocity $V_n = V_e/(M^2 - 1)$, where $M = V_s/a$ is the Mach number of the slowly propagating shock, and $V_s = V_e + V_n$ is the shock speed. (In the limit of high Mach number, $V_s \approx V_e$.) The total width of the slab is then given by the product of this velocity and the age of the slab: $L = 2V_n t$. Note that for high M the slab width grows very slowly compared to L/V_e. Due to the fact that these shocks are isothermal, the compression ratio, defined as the ratio of the slab density to ambient density, is given by $\rho_s/\rho_e = M^2$. We will consider sinusoidal displacements of this slab with an amplitude ζL and wavelength $\lambda = 2\pi/k$, as shown in Figure 1.

The initial conditions within the displaced slab are assumed to be the same as in the steady-state planar slab, namely $v = 0$ and $\rho_s = M^2\rho_e$. While these conditions are not consistent with the shock jump conditions of the perturbed slab under the assumption of steady state, any realistic conditions

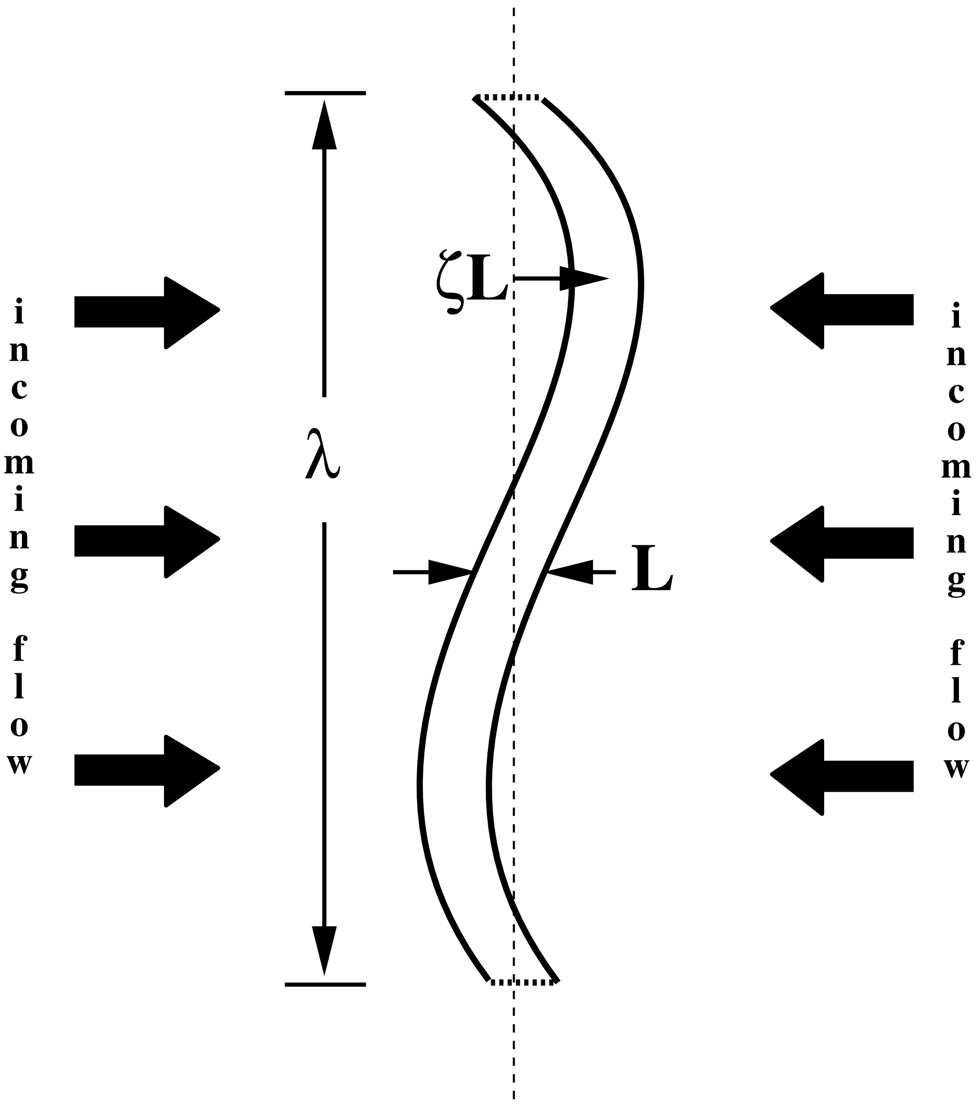

Fig. 1. Schematic of the idealized shock-bounded slab showing the parameters L, ζ, and λ defining the slab perturbation. A uniform flow impinges the slab from both sides with a velocity V_e and density ρ_e.

would require assumptions about the history of the slab, i.e., how did it get perturbed in the first place. We have experimented with other initial conditions and have found that different assumptions of initial flow within the slab do not significantly affect the growth rate of the NTSI. In §3.5 we show an example of the NTSI evolving from realistic, self-consistent initial conditions.

The perturbed slab is evolved on a grid of (typically) 900 by 400 zones, with a resolution of 10 zones across the initial slab width. The hydrodynamic evolution is computed with an isothermal version of VH-1 (http://wonka.physics.ncsu.edu/pub/VH-1), a multidimensional gas-dynamics code based on the piecewise parabolic method developed by Collela & Woodward[0]. The boundary conditions on the left and right sides are fixed at $\pm V_e$, respectively, with a density ρ_e and Mach number M. The top and bottom boundaries are mapped onto each other

Table 1
Parameters for numerical simulations of the NTSI

Model	λ	kL	ζ_i	M	Δ/L
A	45.5	0.138	3.55	25	11
B	20	0.314	1.60	25	10
C	40	0.157	1.60	25	10
D	80	0.078	1.60	25	5
E	20	0.314	1.60	12.5	10
F	20	0.314	1.60	50	10
G	22	0.286	0.33	25	9

creating a periodic grid in the transverse direction. We use normalized values such that the isothermal sound speed $a = 1$ and the initial width of the slab $L = 1$. Unless stated otherwise, the Mach number of the incoming flow is $M = 25$ and the initial displacement is $\zeta_i = 1.6$.

3 Nonlinear Thin-Shell Instability

The analysis of the NTSI by Vishniac[0] suggests that our idealized slab will be unstable to growth of the displacement ζ if $\zeta > 1$ and $kL > M^{-1}$. The former requirement is necessary for growth, while the latter inequality is required to avoid "secular damping" where the normal expansion rate of a planar slab exceeds the growth rate of any perturbations. Vishniac's analysis included a third constraint, namely $kL < 1$ from the assumption of small bending angles. Note that these last two constraints imply the need for a large Mach number in order for a finite range of wavelengths to be unstable.

To study the evolution of the NTSI and its dependencies, we have run many simulations varying the wavelength and amplitude of the initial perturbation, the Mach number of the incoming flow and the numerical resolution. The parameters of six of these simulations, described below, are given in Table 1.

3.1 Initial Evolution

To illustrate the initial growth of the NTSI we begin with a simulation initialized with a relatively large initial perturbation, $\zeta_i = 3.5$ (model A in Table 1). Figures 2, 3, and 4 illustrate the early evolution of this slab, showing the rapid growth of the displacement ζ. As the evolution begins, the incoming flow crossing the bounding shocks is deflected away from the shock normal such

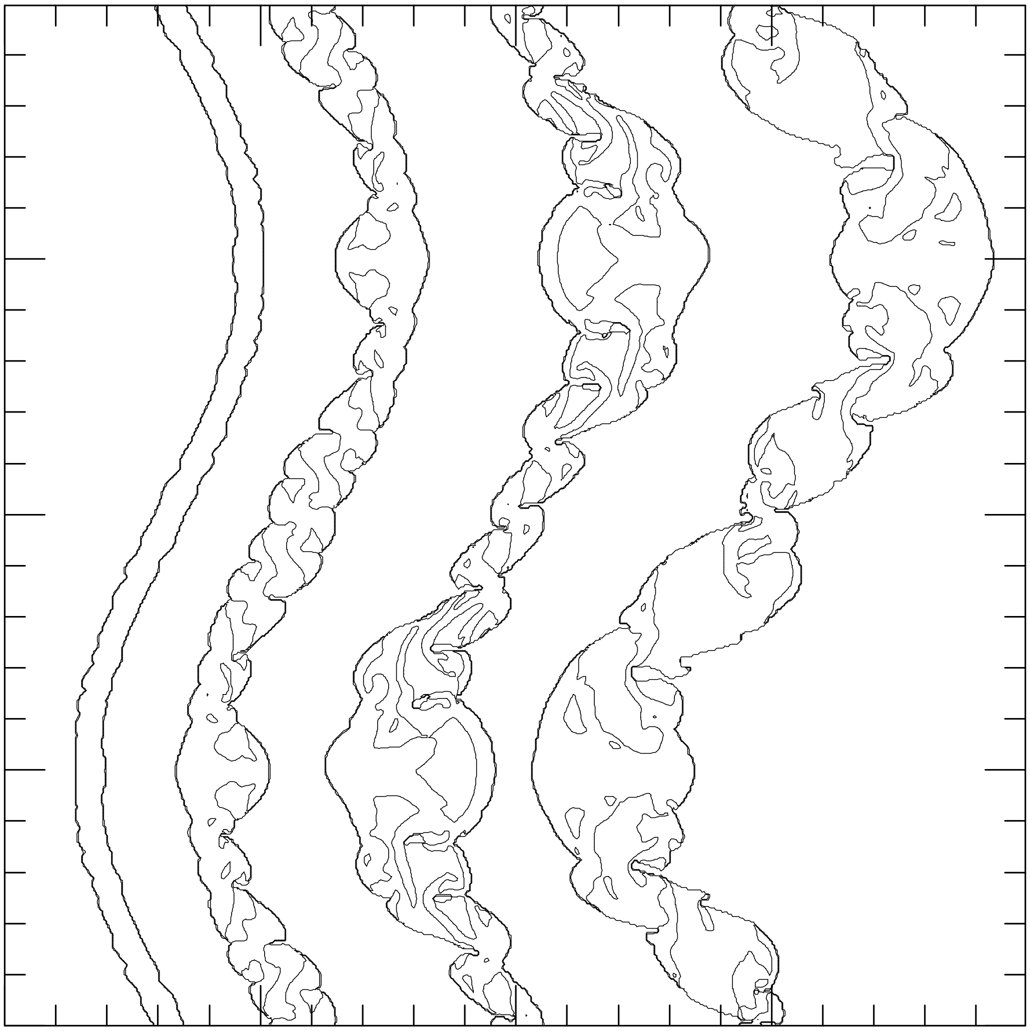

Fig. 2. Early evolution of the NTSI in model A showing the gas density. The unperturbed slab density is $\rho_s = M^2\rho_e = 625\rho_e$. From left to right, the images show the slab at times of 1.95, 4.09, 6.23, and 8.35. The accompanying animation (http://wonka.physics.ncsu.edu/www/ntsi/mAden.mpg) shows the evolution of model A out to a time of 11.4.

that the post shock gas flows parallel to the shock surface. This post shock flow is in a direction that takes it away from the point of maximum deflection in the positive (negative) direction for flow originating from the right (left). The result is a shear flow within the slab, with the gas heading away from the point of maximum deflection on its side. The flow within the slab, while becoming more complicated as the slab evolves, continues to follow this basic pattern. This shear flow is, in fact, the essence of the NTSI: the net transport of positive (negative) momentum in the + (-) direction of inflow due to the obliquity of the perturbed shock fronts.

This net transport and its effects on ζ is clearly seen in 4 (and particularly

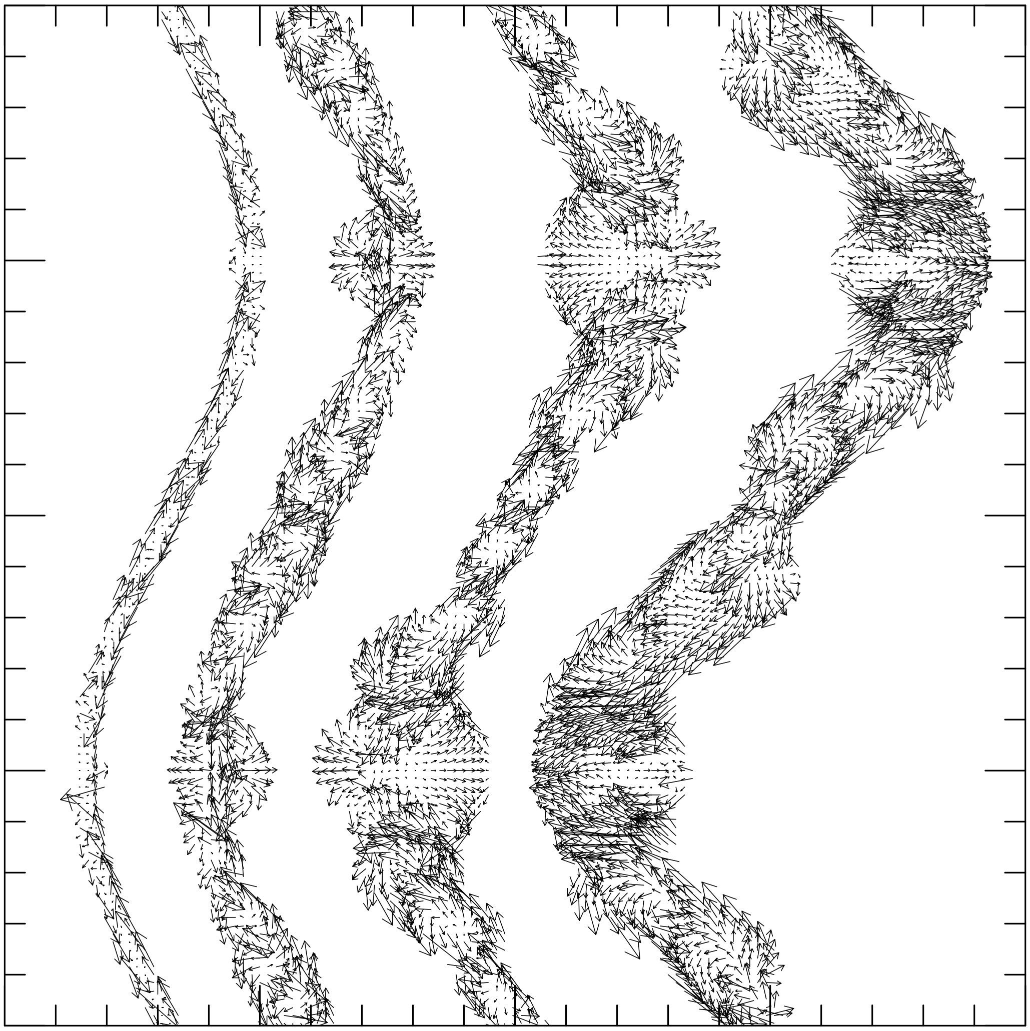

Fig. 3. The velocity field within the slab for the same epochs shown in Figure 2. The longest vector corresponds to a velocity of 7 ($V_e = 25$). The vectors are plotted for every fifth numerical zone in the simulation.

in its accompanying animation), where we plot the momentum in the slab at the same epochs as shown in 2. As the evolution continues, more and more positive (negative) momentum is deposited in the part of the slab with the largest positive (negative) displacement. This flow of momentum drives the extrema of the slab even farther apart; this is the NTSI.

The growth of the slab displacement is shown in Figure 5, where we plot the average of the maximum displacements in the $\pm$ direction as a function of time for three different simulations, all with $M = 25$ and $\zeta_i = 1.6$ but with wavelengths of 20, 40, and 80 (models B, C, and D in Table 1). The analysis of Vishniac[0] suggests that the growth rate will be $\sim (kL)^{3/2}\zeta^{1/2}a/L$. (For our choice of parameters, the characteristic time scale $a/L = 1$.) To show the wavelength dependence on the growth rate, we have plotted lines with slopes

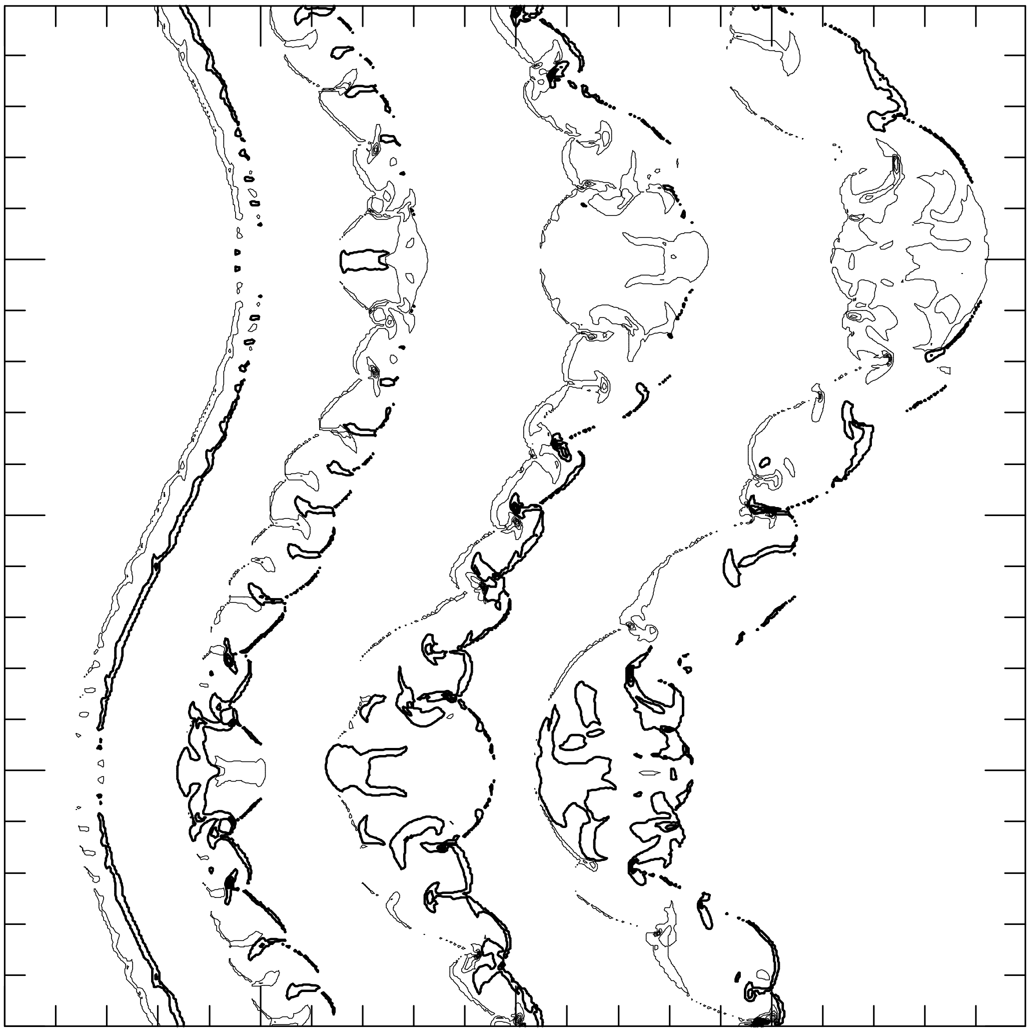

Fig. 4. The distribution of momentum for the same epochs shown in Figure 2. Positive momentum (red; thin contours) accumulates in the displacement to the right, and negative momentum (blue; thick contours) accumulates in the displacement to the left. The accompanying animation (http://wonka.physics.ncsu.edu/www/ntsi/mAmom.mpg) clearly shows the development of the KH instability and its lack of effect on the NTSI.

corresponding to $(kL)^{3/2}$ on Figure 5.

The general trend given by Vishniac, smaller growth rates for larger wavelengths, holds true in the simulations, although the exact dependence on wavelength appears to be weaker than the analytically derived $(kL)^{3/2}$. Furthermore, the growth of ζ in the simulations appears to be exponential, i.e., the growth rate does not depend on the value of ζ. Instead, the growth rate is given approximately by $\tau^{-1} \approx 0.4(kL)^{0.7}$. Note that this approximation is based on a much larger sample of simulations than listed in Table 1. In particular we have confirmed the scaling of the growth rate with a/L, the

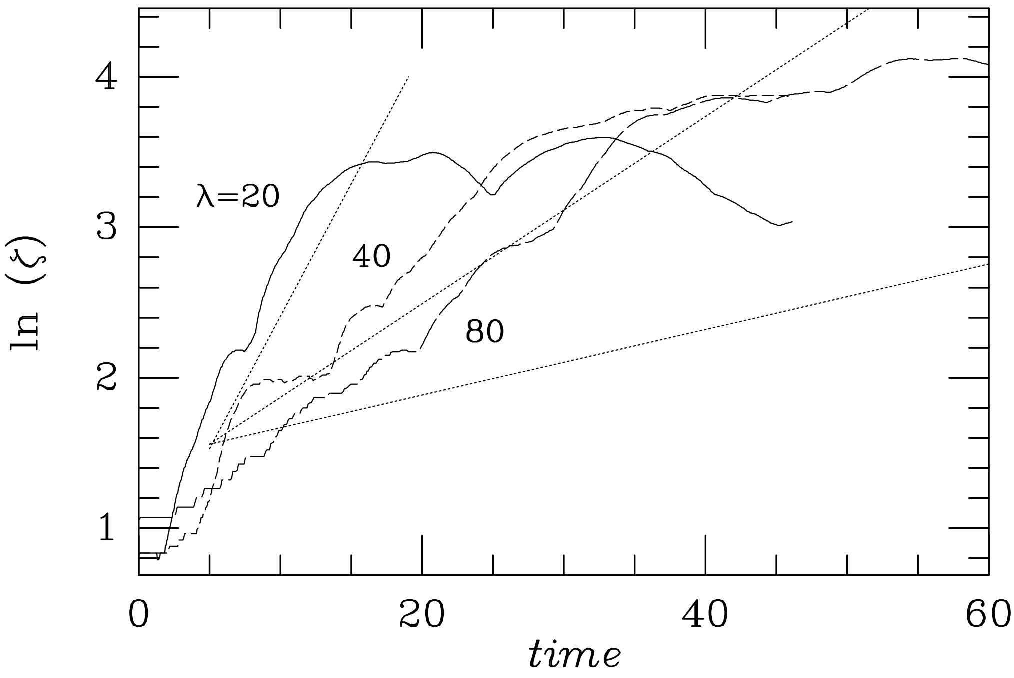

Fig. 5. The growth of the maximum displacement of a shock-bounded slab for three simulations with wavelengths as marked. Each simulation was initialized with $\zeta_i = 1.6$ and $M = 25$. The dotted lines correspond to the lower limit on the growth rate for each run, $(kL)^{3/2}$ as given by Vishniac.

independence of the growth rate on L itself (the dependence is only on the product kL), on ζ_i, and on the Mach number (cf. Figure 7). One should be cautious, however, in drawing conclusions from this data. Given that we are simulating the evolution of a slab in the non-linear regime, there are many competing effects that influence the growth of ζ: the growth of the width of the slab, the inability to isolate a single wavelength, shear instabilities within the slab, and the influence of the ad-hoc initial conditions to name but a few. Nonetheless, the growth of ζ does in fact appear to be exponential, with a growth rate that increases as the value of kL increases.

3.2 Kelvin-Helmholtz Instability

Another feature to note from these simulations is the role of the Kelvin-Helmholtz instability. The obliquity of the shock fronts in the displaced slab leads immediately to a shear flow within the slab as seen in the vector plot in Figure 3 and the animations in Figures 2 and 4. Indeed, it is this shear that is responsible for the growth of the NTSI. This shear flow is expected to be Kelvin-Helmholtz unstable, and our simulations confirm this. From the beginning of the simulation the flow within the slab is affected by the KH instability.

The first modes to appear correspond to $\lambda_{KH} \approx L$, or approximately 30 KH 'rolls' across the NTSI wavelength. This number is slightly dependent on initial conditions and numerical resolution. As the NTSI evolves and the width of the slab increases, so too does the dominant KH wavelength. The result is that λ_{KH} remains of order the current width of the slab. At late times, when the width of the slab has become much larger than the original width, and the interior flow is highly supersonic, the KH instability is essentially absent.

As seen in the simulations of model A (Figures 2, 3 and 4, and particularly the animation accompanying Figure 4), the KH patterns perturb the slab, but do not strongly influence the NTSI. The kinks in the slab generated by the KH can be seen to interact, but for the most part they advect past each other, depositing their momentum in the extrema of the slab as if there was no KH present. This is consistent with the fact that $kL \approx 1$ is the lower limit on unstable wavelengths for the NTSI, and hence one would not expect the KH waves (with $kL < 1$) to excite the NTSI.

The only case where the KH instability appeared to directly affect the NTSI was in our longest wavelength simulation (model D), where the NTSI growth rate was relatively small. In this case the merger of KH rolls generated a perturbation in the slab with kL of order unity, which in turn excited a shorter wavelength mode of the NTSI than the original $\lambda = 80$.

3.3 Saturation

As the NTSI continues to evolve, a strong competing effect can be seen: the growth in the width of the slab (see Figure 6). As the shock fronts become more oblique, the relative shock velocity, and hence shock compression, decreases. In the limit that the relative shock velocity remains highly supersonic (i.e., $V_e \cos\theta \gg a$, where θ is the obliquity of the shock), the boundaries of the slab move with a velocity of $V_n = a^2/(V_e \cos\theta)$. However, now this velocity is at an angle θ with respect to the incoming flow, and in particular the component perpendicular to the incoming flow, $V_n \sin\theta$, acts to "pinch off" the initial perturbation. As the NTSI evolves and the shock obliquity increases, the slab will eventually reach a point where the slab width exceeds half the wavelength, and the NTSI becomes pinched off, as shown in Figure 6. If we equate the time for this lateral velocity to "fill in" the perturbation with the growth time for the NTSI, we arrive at a saturation amplitude for the NTSI of $\zeta_s \approx M_e(kL)^{-1/2}$, where $M_e = V_e/a$. This dependence on λ can be seen in Figure 5, where the maximum value of ζ increases roughly as $\sqrt{\lambda}$. The dependence on Mach number is illustrated in Figure 7, which shows the evolution of ζ for three runs with identical initial conditions except for a difference of a factor of two in the Mach number. The difference in ζ_s is not quite a factor of two between each

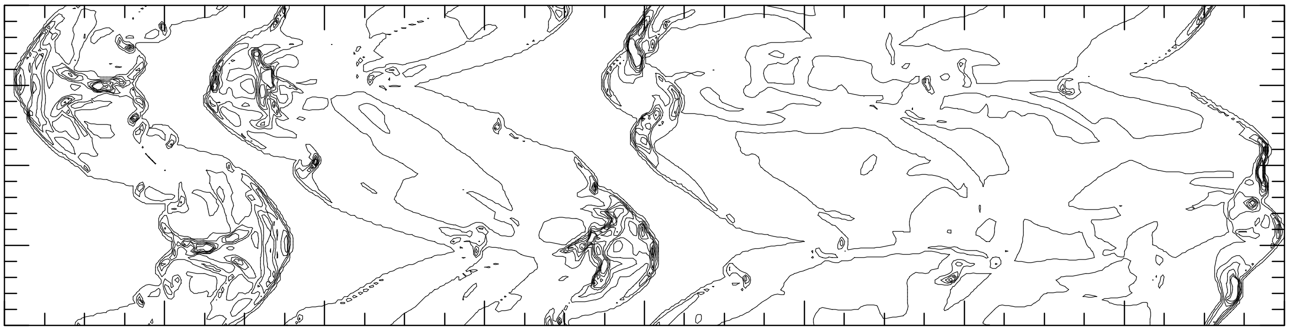

Fig. 6. The saturation of the NTSI in model B due to growth in the width of the slab. The color scale of gas density is the same as in Figure 2. These images corresponding to times of 7.1, 9.4, and 11.7. The accompanying animation (http://wonka.physics.ncsu.edu/www/ntsi/mBden.mpg) shows the evolution of model B out to a time of 27.8.

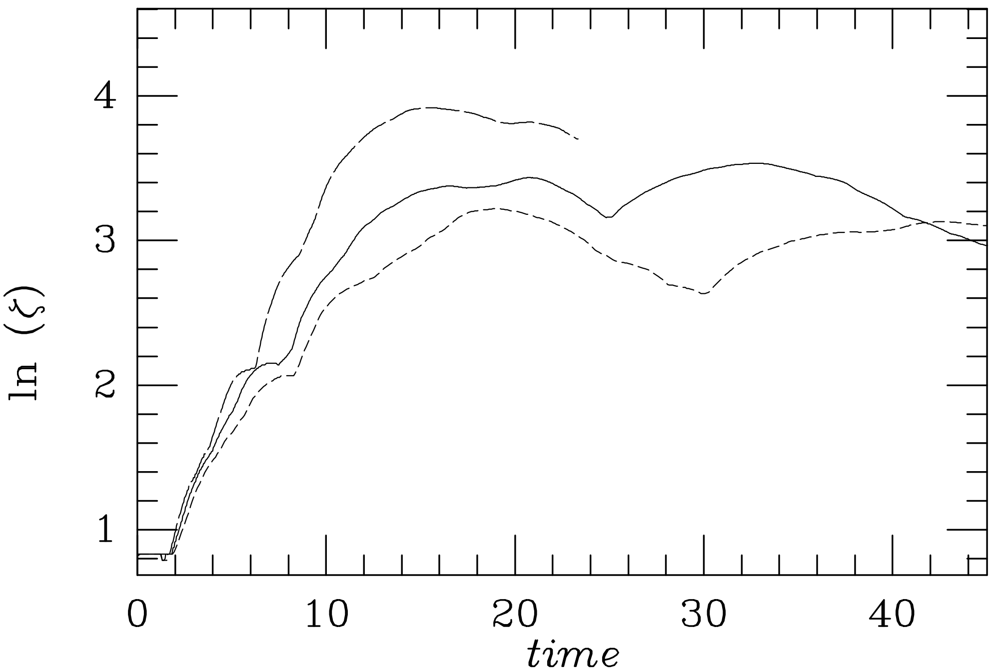

Fig. 7. The growth of the maximum displacement of a shock-bounded slab as a function of Mach number. The three curves are for simulations with identical parameters except for Mach number: M = 12.5 (short dash), 25 (solid), 50 (long dash).

simulation, but the trend is in the right direction. Note again that given the nonlinear nature of this instability, one must be cautious when interpreting results. For instance, initializing a simulation with a different value of ζ_i can have a strong influence on the peak value of ζ.

The growth and subsequent saturation of the NTSI are illustrated in the animation in Figure 6, as well as in a space-time diagram in Figure 8. The length of the image in Figure 8 corresponds to an age of 55.5, by which time a planar slab would have grown to a thickness of 4.5. This is ~ 10 times smaller than the average width of the slab near the end of the simulation. Note from both Figures 5 and 8 and the animations in Figure 6 that the maximum displacement begins to decrease after reaching saturation.

Once the bends are pinched off by the growth of the slab, the shock front is again roughly planar and the shock compression approaches the initial value of M^2. At this point the slab has an average density $\langle\rho\rangle \ll M^2\rho_e$, and is supported internally by supersonic turbulence. This turbulence gradually dissipates as the interior flow continues to shock, and the slab begins to collapse.

In a few of our simulations this post-saturation collapse was quite dramatic, but in most cases the average width of the slab never fell by more than a factor of ~ 2. In these cases the continued deformation of the shock front provided sufficient supersonic turbulence to maintain a highly bloated slab. Furthermore, if a given simulation was rerun on a wider box so as to allow the development of longer wavelength modes, the maximum displacement saturated at a larger value. However, Vishniac[0] quotes a lower limit on kL of M^{-1}, which translates into an upper limit: $\zeta_s < M^{3/2}$ (in the limit of high Mach number). Unfortunately we did not have the computational resources to test this limit.

3.4 Linear Stability

We have also studied the stability of cold, shock-bounded slabs to linear perturbations by initializing a simulation with $\zeta = 0.33$. This is admittedly a rather large value to be considered "linear", but it is small enough that we do not see the vigorous growth associated with the NTSI. However, the slab does not remain thin and laminar, as seen in Figure 9. The initial evolution appears qualitatively similar to simulations subject to the NTSI: a shear flow exciting the KH instability and transporting momentum to the points of maximum displacement. However, in this case the KH instability is able to compete with the NTSI and form smaller wavelength displacements in the slab. These short wavelength displacements quickly fill in as seen in the saturation of the NTSI, with the result that ζ never experiences an exponential growth. Yet, as one can see by comparing Figures 8 and 9, the end state of this simulation (model G) is quantitatively the same as the end state of model B. For comparison, a truly planar slab would have grown to a width of 4.75 by the end of the simulation of model G, compared to an average width of ~ 30 at an age of ~ 47.

Even an initially planar, laminar slab is seen to evolve into a "bloated" tur-

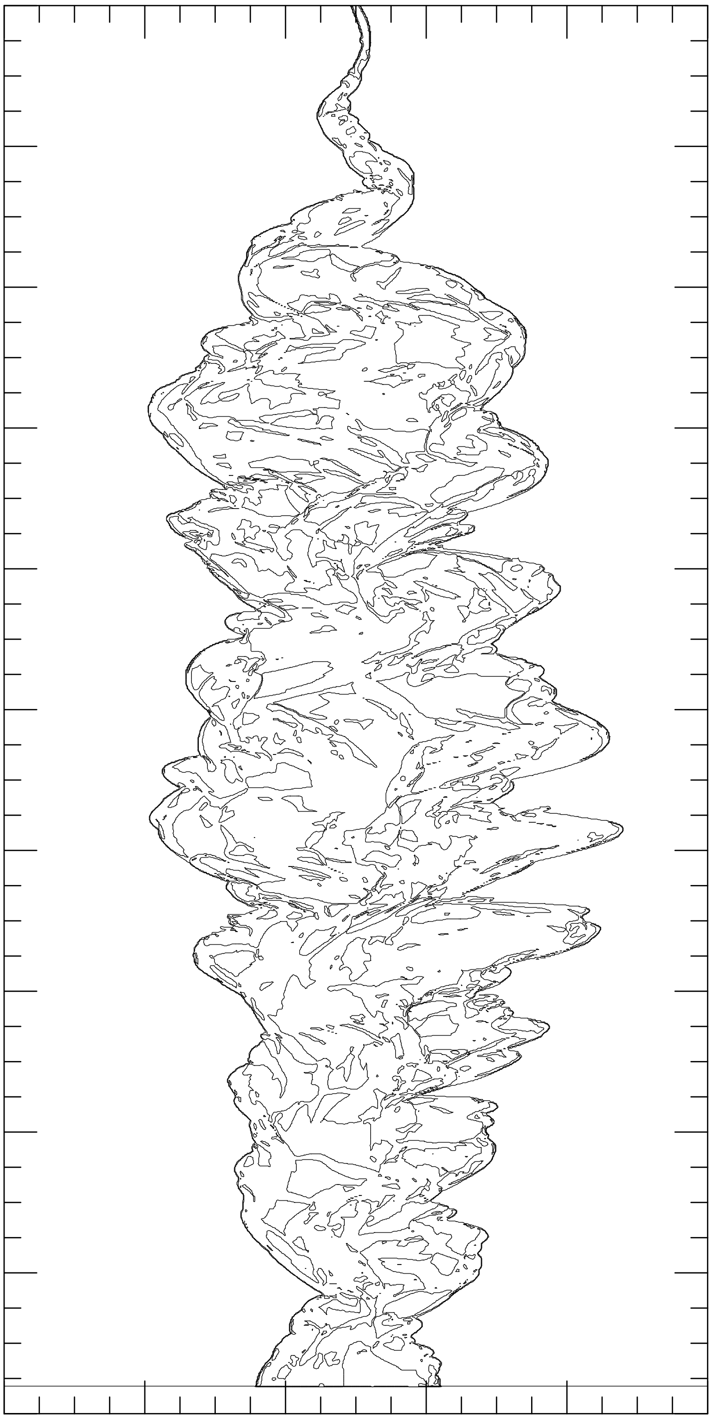

Fig. 8. A space-time diagram illustrating the evolution of the NTSI in model B from nonlinear growth through saturation. The vertical axis represents both time evolution (down the plot) and distance along the slab, while the horizontal axis represents distance perpendicular to the slab. The vertical axis spans a time of 55.5, and the horizontal axis spans a distance of 102. If the slab remained planar, it would have grown to a width of only 4 times the original slab width, corresponding to 4% of the width of the box.

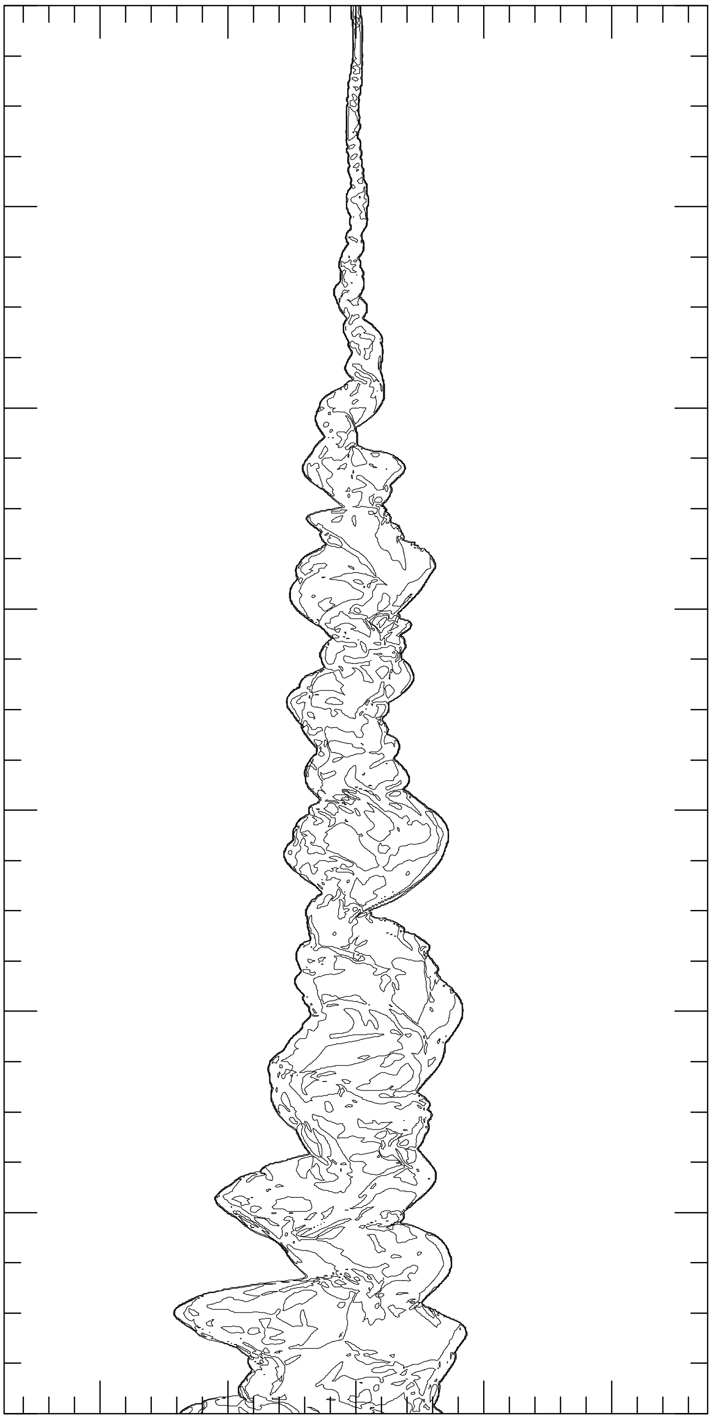

Fig. 9. A space-time diagram and accompanying animation (http://wonka.physics.ncsu.edu/www/ntsi/mGden.mpg) for a shock-bounded slab initialized with a small perturbation, $\zeta = 0.33$ (model G). The width of the box spans a distance of 100, and the length spans a time of 47. Although this slab does not show the rapid growth associated with the NTSI seen in Figure 8, it does not remain laminar; the average width at the end of the simulation is ~ 7 times larger than if the slab had remained planar (i.e., compared to $L = 2V_n t$).

bulent slab as a result of small numerical noise generated in the strong shock fronts, although the width does not greatly exceed that of a laminar slab (see Figure 10). While the origin of this effect is numerical noise, one would expect such small perturbations (of order 1%) in a realistic environment. If we increased dissipation in our hydrodynamic code, decreasing the magnitude of the post-shock noise, the transition from laminar to turbulent was delayed but never prevented. Thus, while the NTSI does indeed appear to be a nonlinear phenomenon, a planar slab with laminar interior flow does not appear to be stable. This result may correspond to the two-dimensional hydrodynamic simulations of radiative shocks by Strickland & Blondin[0], in which they find that the cold, post shock gas is never laminar.

3.5 Realistic Initial Conditions

As we described earlier, the initial conditions of a perturbed slab with $v = 0$ inside the slab are inconsistent. When we included a post shock flow in an attempt to create a self-consistent perturbed slab, the NTSI "took off" even faster, as one might expect. However, one might ask how these initial nonlinear displacements occurred in the first place. One possible answer to this question is: something hit the slab with enough momentum to displace it. In Figure 11 we show the evolution of the NTSI after a small cloud impacts a planar slab. (Given the planar geometry of this simulation, the cloud is actually an infinitely long cylinder.) The width of the cloud is five times the width of the initial stationary slab, and the density is ten times the ambient density (compared to the slab density of $625\rho_e$). We have run simulations with different cloud sizes, and find that the NTSI is excited as long as the cloud radius is more than the width of the cloud (to satisfy $kL < 1$) and the column density of the cloud, $n_c R_c$, is at least 5% of the column density in the slab (to ensure a displacement larger than the width of the slab).

Immediately after impact a small length of the slab is displaced in the direction of the motion of the cloud. Provided that this initial displacement is at least as large as the width of the slab, we have the conditions for the NTSI. In this particular simulation the initial displacement, which resembles a bow shock, deflects shocked flow impinging from the right, away from the head of the bow shock and towards the unperturbed slab. The excess negative momentum from this interior flow pushes the unperturbed slab at the wings of the bow shock, driving displacements into the incoming flow from the left, forming the shape of a "W". The two new extrema extending into the left hand flow now redirect positive momentum in a similar fashion to the original extremum. In this fashion the NTSI propagates down the length of the slab.

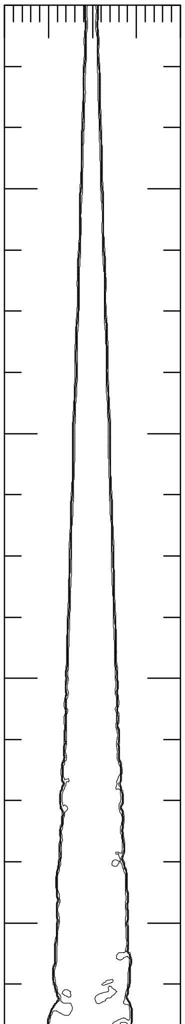

Fig. 10. A space-time diagram for an initially planar slab evolved to an age of 115 (considerably longer than in Figure 9). The width of the plot in units of L is 20. Eventually numerical postshock noise excites instabilities in the slab disrupting the laminar flow, although the average density of the slab remains relatively high.

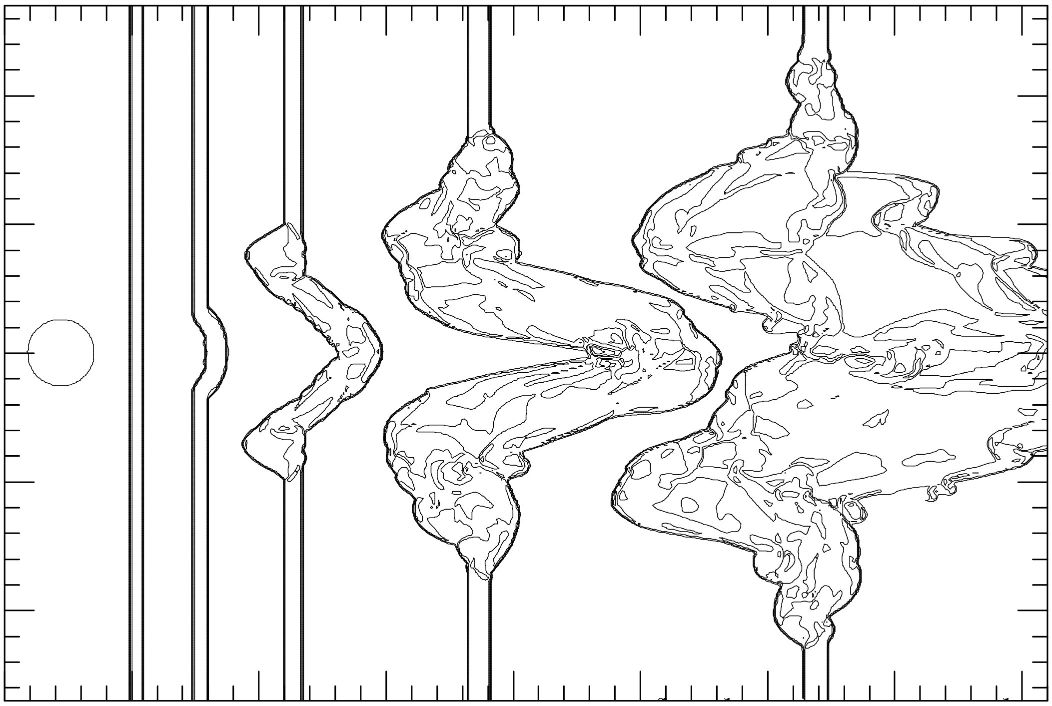

Fig. 11. Evolution of a shock-bounded slab impacted by a small cloud. The density of the slab is shown just prior to impact, and at times after impact of 1.1, 4.3, 8.0, and 10.6. Once the NTSI is excited by the cloud impact, it propagates down the length of the slab, disrupting the entire slab. The accompanying animation (http://wonka.physics.ncsu.edu/www/ntsi/cloud.mpg) shows the full evolution out to a time of 12.

4 Discussion

The simulations of shock-bounded slabs described in this paper suggest that such slabs are inherently unstable provided the incoming flow is sufficiently supersonic. Rather than existing as a thin, roughly planar slab with an approximate density of $\rho_s = M^2\rho_e$ and width $L = 2V_n t$, one should expect the interaction region between colliding, isothermal supersonic flows to consist of two highly irregular shock fronts separated by an average distance much greater than L. The separation of the shock fronts is supported by supersonic turbulence, which generates an interior marked by numerous thin, dense filaments.

The NTSI is even more robust in the case of colliding stellar winds, as seen by Stevens et al.[0], presumably because of the divergent flow geometry. In this case the spherically diverging stellar wind advects the perturbations downstream, stretching out their wavelengths in the process. As a result, the NTSI does not get pinched off as in the planar case, and the instability appears to grow unbounded. This same effect may happen in the case of stellar wind bow shocks analyzed by Dgani, Van Buren, & Noriega-Crespo[0], which is geometrically similar to the colliding winds case. While these authors argue that another instability that they refer to as the transverse acceleration instability (TAI) will dominate in such bow shocks, the exact role of the TAI and NTSI must await accurate numerical simulations.

Another example of the NTSI in a spherically diverging geometry is in time dependent stellar winds[0]. These authors modeled the evolution of the stellar wind of a $60 M_{\odot}$ star. During the luminous blue variable (LBV) stage, a slow ($v_{\infty} \approx 300\,\mathrm{km\,s^{-1}}$), dense ($\dot{M} > 10^{-4} M_{\odot}\mathrm{yr}^{-1}$) wind forms a thin wind-swept shell bounded on both sides by radiatively cooling shocks. This situation differs from a typical stellar wind bubble in that the very high density of the LBV wind leads to a radiative terminal wind shock as well as a radiative outer shock. In the simulations of Garcia-Segura et al.[0], this thin shell is quickly rippled, presumably due to the NTSI.

The work of Anninos et al.[0] on the evolution of cosmological sheets shows the rippling of a layer of cold gas in the middle of an accreting slab. This is not the NTSI, for the cold slab is enclosed within a larger slab of shock-heated gas. In this case the post shock cooling length behind the accretion shocks is larger than the width of the cold slab. The instability of the cold gas layer seen in their simulations is instead related to the instabilities seen by Strickland & Blondin[0] in their studies of radiative shocks. If the parameters of the sheet formation were such that $L_{cool} \ll L_{slab}$, then the NTSI would be applicable to this problem.

5 Conclusion

We have used numerical hydrodynamics simulations to confirm the presence of the nonlinear thin-shell instability. If the position of a cold, shock-bounded slab is displaced by a distance larger than the width of the slab, the displacement will grow with an exponential rate of $\tau^{-1} \approx 0.4(kL)^{0.7}$. We find that the NTSI saturates when the growth in the width of the slab exceeds the NTSI growth rate and the perturbations are “filled in”. The maximum width of the slab at saturation is $\zeta_s \approx M_e (kL)^{-1/2}$. While linear perturbations do not grow exponentially as in the NTSI, they do lead to a bloated slab supported internally by supersonic turbulence generated by non-planar shock fronts.

Acknowledgement

This research was supported in part by NASA grant NAG 5-2844. B.S.M. acknowledges support from the NSF Research Experiences for Undergraduates program funded through the American Astronomical Society. The numerical simulations described in this paper were computed on a Cray T90 at the North Carolina Supercomputing Center.

References

[1] Anninos, W. Y., Norman, M. L., & Anninos, P. 1995, ApJ, 450, 1.

[2] Blondin, J. M., Wright, E., Borkowski, K. J., & Reynolds, S. P. 1996, ApJ, submitted.

[3] Colella, P., & Woodward, P. R. 1984, J. Comp. Phys., 54, 174.

[4] Dgani, R., Van Buren, D., & Noriega-Crespo, A. 1996, ApJ, 461, 927.

[5] Garcia-Segura, G., Mac Low, M.-M., & Langer, N. 1996, A&A, 305, 229.

[6] Hunter, H. H., Sanford, M. T., Whitaker, R. S., & Klein, R. I. 1986, ApJ, 305, 309.

[7] Murray, S. D., & Lin, D. N. C. 1989, ApJ, 339, 933.

[8] Stevens, I. R., Blondin, J. M., & Pollack, A. M. T. 1992, ApJ, 386, 265.

[9] Strickland, R., & Blondin, J. M. 1995, ApJ, 449, 727.

[10] Vishniac, E. T. 1994, ApJ, 428, 186.